Epitaxial Graphene on 4H-SiC(0001) Grown under Nitrogen Flux: Evidence of Low Nitrogen Doping and High Charge Transfer

Emilio Velez-Fort,[†,‡] Claire Mathieu,[†] Emiliano Pallecchi,[†] Marine Pigneur,[†] Mathieu G. Silly,[§] Rachid Belkhou,[§] Massimiliano Marangolo,[⊥] Abhay Shukla,[‡] Fausto Sirotti,[§] and Abdelkarim Ouerghi[†,*]

[†]Laboratoire de Photonique et de Nanostructures (CNRS-LPN), Route de Nozay, 91460 Marcoussis, France, [‡]Université Pierre et Marie Curie (CNRS-IMPMC), 4 Pl. Jussieu, 75005 Paris, France, [§]Synchrotron-SOLEIL, Saint-Aubin, BP48, F91192 Gif sur Yvette Cedex, France, and [⊥]Institut des NanoSciences de Paris, UPMC-CNRS, UMR 7588, 4 Pl. Jussieu, 75005 Paris, France

ABSTRACT Nitrogen doping of graphene is of great interest for both fundamental research to explore the effect of dopants on a 2D electrical conductor and applications such as lithium storage, composites, and nanoelectronic devices. Here, we report on the modifications of the electronic properties of epitaxial graphene thanks to the introduction, during the growth, of nitrogen-atom substitution in the carbon honeycomb lattice. High-resolution transmission microscopy and low-energy electron microscopy investigations indicate that the nitrogen-doped graphene is uniform at large scale. The substitution of nitrogen atoms in the graphene planes was confirmed by high-resolution X-ray photoelectron spectroscopy, which reveals several atomic configurations for the nitrogen atoms: graphitic-like, pyridine-like, and pyrrolic-like. Angle-resolved photoemission measurements show that the N-doped graphene exhibits large n-type carrier concentrations of 2.6×10^{13} cm^{-2}, about 4 times more than what is found for pristine graphene, grown under similar pressure conditions. Our experiments demonstrate that a small amount of dopants (<1%) can significantly tune the electronic properties of graphene by shifting the Dirac cone about 0.3 eV toward higher binding energies with respect to the π band of pristine graphene, which is a key feature for envisioning applications in nanoelectronics.

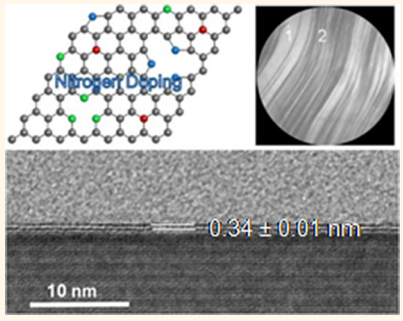

KEYWORDS: epitaxial graphene · spectroscopy · nitrogen-doped · low-energy electron microscopy · electronic properties

Graphene is a single layer of carbon atoms arranged in a honeycomb structure.[1] Its extraordinary properties, such as high carrier mobility up to room temperature, half-integer quantum Hall effect, weak electron−phonon coupling, and long spin coherence time,[2,3] have made graphene a very promising candidate as a robust atomic-scale scaffold in the design of new nanomaterials.[4,5] In addition to its physical properties, the interest for this material is driven by the promise of applications to novel graphene-based devices such as field effect transistors (FET), transparent electrodes, supercapacitors, and lithium ion batteries.[6,7] For these purposes, modifications of the electronic properties are required. For instance, a band gap opening is crucial for achieving FETs with a high on/off ratio, and a low sheet resistivity is necessary for application to transparent electrodes.[8,9]

Chemical doping is one of the most promising ways to tailor the properties of graphene. The substitution of carbon atoms in the honeycomb lattice by atoms with a different number of valence electrons will, in general, affect the density of states (DOS) of the graphene. Whether these will introduce electron-donor states, electron-acceptor states, or neither of these two depends crucially on the local bonding arrangements of the heteroatoms.[10−14] Particularly, nitrogen doping plays a critical role in regulating the electronic and chemical properties of carbon materials due to its comparable atomic size. Theoretical and experimental studies have indicated that the chemical properties of nitrogen-doped graphene, such as dopant density and the bonding configuration can

* Address correspondence to abdelkarim.ouerghi@lpn.cnrs.fr.

Received for review September 18, 2012 and accepted November 13, 2012.

Published online November 13, 2012
10.1021/nn304315z

dramatically change its physical properties, such as the electronic and magnetic characteristics.[15−18]

Recently, several postgrowth doping approaches have been successfully demonstrated. The most common is thermal annealing of graphene oxide in ammonia.[19−22] Moreover, low-energy nitrogen ion irradiation has proven to be a useful tool for doping the carbon network with controlled doses.[5] Concerning the *in situ* doping, that is, during the graphene growth, the chemical vapor deposition (CVD) on metal substrates of N-doped graphene obtained with NH_3 as a precursor was also reported.[23] For electronic applications, the growth of graphene by CVD on metals requires transferring the graphene onto an insulating substrate. This transfer step is not yet fully mastered and involves heavy chemical manipulations, which can lead to sample contaminations.

On the other hand, epitaxial graphene on hexagonal silicon carbide (SiC) wafers, which is known to produce homogeneous films with large areas under argon flux,[24] can be used without any transfer. The SiC substrate is suitable for opto-electronic applications since it is transparent over a very broad frequency spectrum, has a large thermal conductivity, and is compatible with high-frequency devices where losses due to residual conductivity of the substrate have to be minimized by using insulating materials. However, to our knowledge, only one work by Joucken *et al.* focused on nitrogen doping of epitaxial graphene.[25] The authors have doped postgrowth the graphene with a radio frequency plasma source fed with N_2 and performed scanning tunneling microscopy and scanning tunneling spectroscopy to investigate the properties of nitrogen-doped graphene.

Here, we describe a method to grow *in situ* N-doped epitaxial graphene on 4H-SiC(0001) by exposing the substrate to nitrogen gas during the graphene growth. The homogeneity of the as-grown layers was confirmed by high-resolution transmission electron microscopy (HR-TEM), and the graphene film was characterized by Raman, X-ray, and angle-resolved photoemission spectroscopy (XPS and ARPES). To highlight the effect of nitrogen doping, these measurements were compared with results obtained on pristine graphene, that is, grown without the nitrogen flow. From XPS, we identify the nitrogen concentration for the different bonding configurations, and from ARPES, we obtain the carrier concentration. Our results show that the substitution of a small amount of carbon by N atoms preserves the linear dispersion of graphene and significantly shifts the Dirac point toward the higher binding energy.

RESULTS AND DISCUSSION

Thermal decomposition of a undoped 4H-SiC(0001) can be used to produce large graphene films with a high long-range order by combining N_2 and Si fluxes during the graphitization.[26] Monolayer, bilayer, and few-layer graphene on SiC can also be obtained by tuning the different experimental parameters (temperature, annealing times, Si flux).[27] We synthesized two N-doped graphene samples by exposing the 4H-SiC substrates to N_2 and Si fluxes at a pressure of 2×10^{-5} mbar during 10 and 15 min (see Methods section). After growth, the samples were cooled to 600 °C under N_2 atmosphere. The first sample has been used for low-energy electron microscopy (LEEM), low-energy electron diffraction (LEED), and HR-TEM experiments and presents about 1.5 monolayer (ML). The second sample has been used for photoemission experiments and is about 0.8 ML. As a reference, a "standard" epitaxial graphene on 4H-SiC(0001) was also synthesized using argon, under the same pressure conditions. This sample will be named hereafter "pristine graphene".

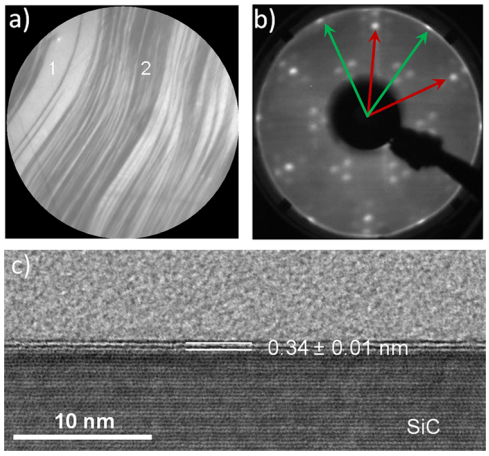

Figure 1. Morphological and diffraction surface of graphene/4H-SiC(0001). (a) Typical LEEM image of the sample showing that the layer coverage is one (bright) and two (dark), predominantly on this sample. The electron energy used is E_{vac} + 4.0 eV and the FOV 50 μm. (b) LEED pattern at 120 eV. (c) Cross-sectional high-resolution TEM image of N-doped graphene.

Figure 1 presents LEEM, LEED, and HR-TEM images obtained on the N-doped graphene sample. Figure 1a shows a LEEM image, in which the contrast highlights the spatial thickness distribution of the sample. Monolayer and bilayer graphene can be unambiguously attributed, thanks to their different behavior in the electron reflectivity curves.[24] The sample is uniformly covered by a graphene monolayer (light gray) on which a ribbon-shaped graphene bilayer can be observed (dark gray). Typically, these ribbons are 5 μm wide, 500 μm long, and are all aligned along the ⟨1−100⟩ SiC axis. It is worthwhile to notice that the lateral size of these ribbons is much larger than the underlying step distance of the substrate (500 nm), indicating that the graphene covers the step edge.[25] The corresponding low-energy electron diffraction (LEED) pattern (Figure 1b) includes two contributions. The first, arising from the sharp (1 × 1) graphene layer (green arrows), confirms the presence of a homogeneous surface and uniform in-plane orientation of graphene with respect to the

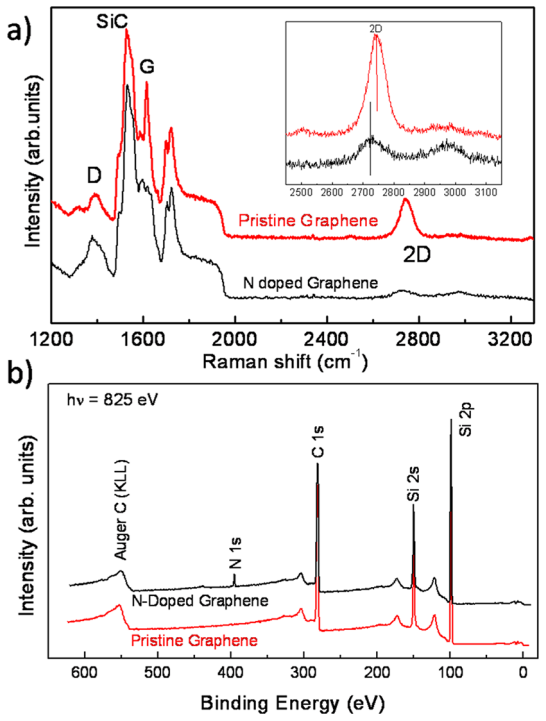

Figure 2. (a) Comparison of micro-Raman spectra taken on the pristine (red line) and nitrogen-doped graphene (black line) layer. Inset: Zoomed image of the 2D Raman region. (b) XPS spectra of the pristine graphene (red line) and the N-doped graphene (black line).

substrate (red arrows).[24,27] The second one, which is characterized by isotropic (circular) 1/6 fractional spots, is attributed to the $(6\sqrt{3} \times 6\sqrt{3})R30°$ reconstructed layer.

In order to investigate the interface, cross-sectional HR-TEM experiments were performed on N-doped epitaxial graphene. This cross-sectional view was observed along the (11−20) SiC zone axis. HR-TEM images reveal the thickness of the graphene layers and the detailed crystalline structure of the N-doped graphene (Figure 1c). As observed from the HR-TEM images, the N-doped graphene grown on SiC, produced here, is predominantly composed by monolayers and bilayers. The interlayer separation is about 0.34 ± 0.01 nm, the graphitic layers are atomically flat and form a continuous film.

All previous experiments were performed on N-doped graphene, but the differences with respect to pristine graphene layers are not discussed because the presence of nitrogen cannot be clearly detected using these techniques. In order to probe the effects of nitrogen dopants on the vibrational and electronic properties of the graphene layer, we performed micro-Raman spectroscopy on the second N-doped and on the pristine samples. Figure 2a compares the Raman spectrum of the pristine graphene (red line) and the one of N-doped graphene (black line) in the wavelength range of 1200−3000 cm^{-1}. Several intense peaks are observed between 1200 and 1800 cm^{-1}; they correspond to second-order Raman bands originated in the SiC substrate.[28] Graphene contributions are also observed, as expected on the pristine sample, they are identified by three main structures: (i) the D band at 1355 cm^{-1}, (ii) the G band at 1595 cm^{-1}, and (iii) the 2D band at 2720 cm^{-1}. For pristine graphene, the D peak is weak, indicating the low density of defects.

In the case of N-doped graphene, we note one more contribution due to the (G+D) bands at 2930 cm^{-1}, corresponding to the disorder-induced feature, which is known to occur in sp^2 carbon with defects. The high intensity of the D band, as well as the presence of the (G+D) band, suggests the incorporation of nitrogen atoms as heteroatoms that break the symmetry of the graphene lattice.[28−30] The I_D/I_G ratio for N-doped graphene represents the degree of disorder within the graphitic carbon, which is estimated in our data to be 0.6 after the SiC background subtraction. The in-plane crystallite sizes (La) of the N-doped graphene are calculated using the following formula:[32] $La = 560/(E_{laser})^4(I_D/I_G)^{-1}$, where, E_{laser} is the Raman excitation wavelength, and I_D and I_G represent the relative intensity of D and G bands. This gives an estimated crystallite size of about 50 nm.

The micro-Raman spectra in the 2D band range, obtained for pristine graphene (red line) and for the N-doped graphene (black line), are compared in the inset of Figure 2a. In this figure, the pristine 2D line is *more* blue-shifted than the doped 2D line, which would imply that the shifts are due to compressive strain rather than doping since doping would provoke the opposite effect. A similar observation for the G line would confirm this hypothesis, but in our data, the G line signal is not strong enough.

To investigate the atomic composition as well as the chemical bonding environment of our samples, XPS measurements were carried out for the N-doped and pristine graphene, as shown in Figure 2b. The XPS measurements performed on a wide energy range show that the C 1s, Si 2s, and Si 2p peak intensities are not notably affected by the presence of nitrogen (Figure 2b) whose presence is confirmed by the N 1s core level peak observed on the N-doped graphene layer. No other element is detected in our spectra. The absence of O 1s signal in the XPS spectra validates that the oxygen contamination has been completely removed by the annealing at 600 °C, performed before all measurements, under UHV conditions.

Different components contributing to the spectra were decomposed by a curve-fitting procedure. The depth position of the corresponding species within the surface was identified by varying the incident photon energy and thus changing the surface sensitivity for Si 2p N-doped graphene. The experimental data points are displayed as dots. The solid line is the envelope of the fitted components. The C 1s core level spectra of

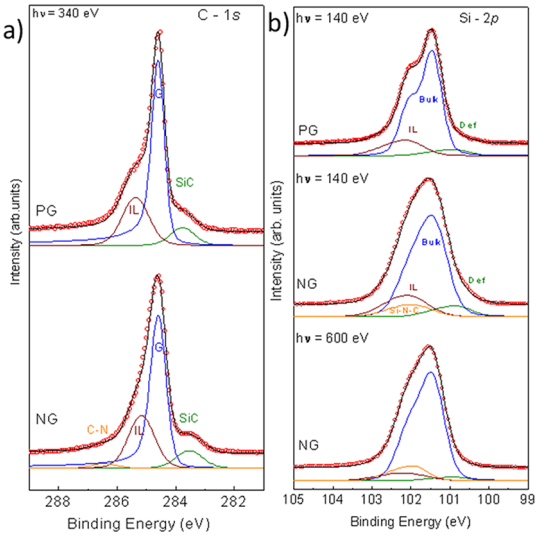

Figure 3. (a) C 1s XPS spectra for pristine (top panel) and N-doped graphene (bottom panel) at $h\nu$ = 340 eV (surface sensitive). The spectra were fitted using a Doniach–Sunjic line shape analysis. (b) Si 2p XPS spectra for pristine and N-doped graphene at $h\nu$ = 140 eV (surface sensitive, top and middle panel) and Si 2p spectra at $h\nu$ = 600 eV (bulk sensitive, bottom panel). XPS measurements were performed at φ = 90° emergency angle with respect to the sample normal.

pristine (top panel) and N-doped graphene layer (bottom panel) are compared in Figure 3a. The spectrum of pristine graphene presents the typical shape of a graphene monolayer grown on SiC(0001). It is composed by three contributions attributed to the SiC substrate (SiC), the graphene layer (G), and the interface layer (IL).[24,26] The C 1s spectra of the nitrogen-doped graphene can be decomposed into four peaks at 283.5, 284.6, 285.2, and 286.5 eV, which can be assigned to SiC, G, IL, and C–N bonds, respectively. The small new peak at 286.5 suggests the bonding formation of doped nitrogen atoms to be sp^2-C or sp^3-C atoms, respectively.[7] Compared with the pristine graphene, the high-resolution C 1s (SiC) and C 1s (IL) peaks of N-doped graphene shift to lower binding energy and the full width at half-maximum (fwhm) of C 1s (G) at 284.6 eV (fwhm = 0.6) increases in comparison with pristine graphene (fwhm = 0.5). All of these results indicate the formation of C–N bonds in the N-doped sample.

Figure 3b shows the Si 2p spectra for nitrogen-doped (middle and bottom panel) and pristine epitaxial (top panel) graphene. The Si 2p peaks are made up of spin–orbit split doublets, and the binding energies are given with respect to the Si $2p_{3/2}$ position. Both spectra consist of a dominant Si 2p peak at 101.5 eV. The small shoulder at 102.1 eV is attributed to the interface layer area of the SiC(0001) substrate, while the component at 100.9 eV is attributed to the presence of Si clusters formed when Si–C bonds are broken during graphitization.[31]

For the nitrogen-doped graphene spectrum, we measure an additional Si 2p component at a higher binding energy (101.9 eV) due to Si–N–C bonds.

At lower photon energy (140 eV, middle panel) where the surface sensitivity is higher, this signal is weak, whereas it becomes stronger at higher photon energy or less surface sensitive conditions (600 eV, bottom panel). We notice that this component increases when the photon energy is tuned to less surface sensitive conditions. This indicates that nitrogen penetrates into the silicon carbide substrate. This implies that the graphene layer, the graphene/SiC interfacial region, and the SiC substrate can all be modified under N_2 flux with notably a nitrogen-passivated SiC region between the N-doped graphene layer and the SiC substrate.[33,34] Moreover, the nitrogen atoms which penetrate into the substrate may introduce disorder which can explain the widening of the bulk Si 2p component for the nitrogen-doped sample (Figure 3b).

Figure 4a shows the N 1s spectra for the N-doped graphene sample. In this high-resolution spectrum, recorded for two photon energies (480 and 600 eV), we can identify four peaks. The N 1s peak components at 397.7 (N1), 398.0 (N2), 400.9 (N3), and 401.9 (N4) eV have been assigned to Si–N–C bonds, pyridinic-N (N bounded to two C), pyrrolic-N (N included in a C pentagon ring connected to two C), and graphitic-N (N linked to three C), respectively (Figure 4b,c). We find that for lower photon energies (higher surface sensitivity) the N2, N3, and N4 components are stronger. This observation is important since these surface contributions are a fingerprint of the effective graphitic nitrogen in the graphene layer.

The binding energy of N in Si–N–C configuration and of pyridinic-N is known to be similar. Disentangling their contributions is not straightforward. In our deconvolution procedure, we assigned the binding energy of 397.7 eV to Si–N–C chemical states, as well as a second peak at 398.0 eV associated with nitrogen bonded in the nongraphitic configuration because the Si 2p spectra imply the presence of the first species and step edges imply the presence of the second. For example, in pyridinic or pyrrolic graphene, one of the carbon atoms is removed (vacancy) from the honeycomb lattice to form step edges. Previously, in the case of N-doped graphene grown by CVD, Wei *et al.* have attributed these peaks to pyridinic doping environments.[23] It has been reported that the interface is a warped carbon layer with periodic inclusions of pentagon–hexagon–heptagon complexes covalently bonded to the Si atoms of the substrate.[35] The presence of defects in the interface layer facilitates the incorporation of the nitrogen atoms through different configurations, involving the formation of Si–N–C bonds and Si–N at the interface layer and eventual modification of charge transfer between the substrate and graphene.

From photoemission spectra, we can estimate the nitrogen concentrations at the sample surface.

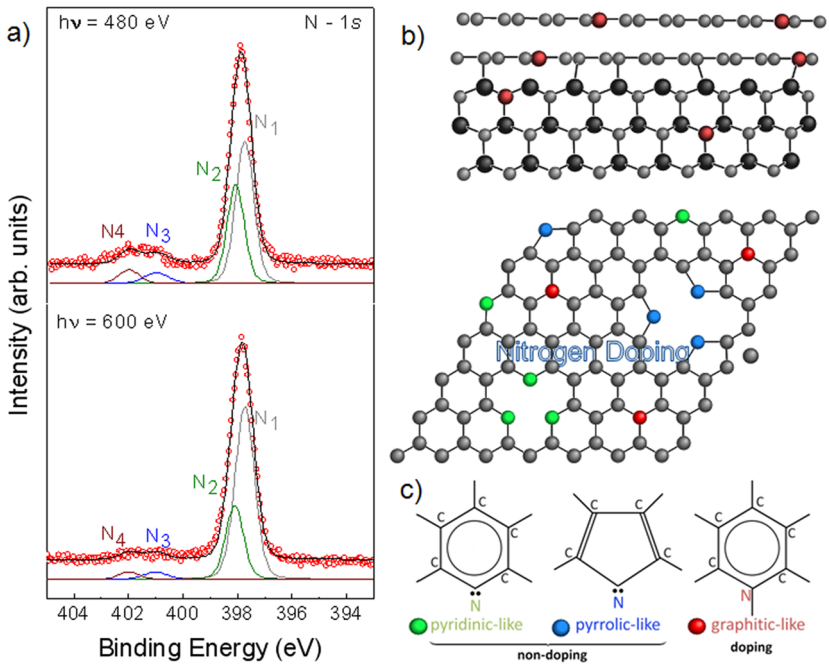

Figure 4. (a) High-resolution N 1s spectra of the nitrogen-doped graphene at $h\nu = 480$ eV (surface sensitive, top panel) and N 1s at $h\nu = 600$ eV (bulk sensitive, bottom panel). (b) Sketch of nitrogen-doped graphene with the four suggested doping sites, *i.e.*, graphitic, pyrrolic, and pyridinic nitrogen, and Si−N formation (side and top view). (c) Different configurations of N-doped graphene layer.

The total amount of nitrogen atoms can be calculated from the N 1s and C 1s peak area ratio in the surface sensitive configuration weighted by the relative cross sections.[36] The total amount of N atoms can then be distributed at various depths in the sample accordingly to the binding energies. The nitrogen atoms in pyridinic, pyrrolic, and graphitic configurations correspond to 4, 0.6, and 0.6% of the carbon atoms in the graphene and interface layer. In particular, graphitic nitrogen atoms were assumed to dope uniformly the deeper graphene layer. The N 1s peak associated with pyridinic and graphitic nitrogen shifts toward higher binding energy in comparison with CVD-grown N-doped graphene.[23] This can be explained by the different chemical environment of the graphitic and pyridinic nitrogen (presence of oxygen), substrate interaction, and the presence of an interface layer.[13,14]

To gain further insight into the electronic properties of the N-doped graphene layer, we performed near-edge X-ray absorption fine structure (NEXAFS) experiments on the same set of samples. It is well-known that NEXAFS can be applied to explore the bond orientation of planar π-conjugated molecules adsorbed on a surface.[36] The spectra were collected by monitoring the carbon Auger peak in order to enhance the surface (graphene) contribution with respect to the SiC substrate.

Recently, it was widely used to study the polarization dependence of the π and σ resonances for graphene and functionalized graphite. The normalized C 1s NEXAFS spectra for pristine and N-doped graphene

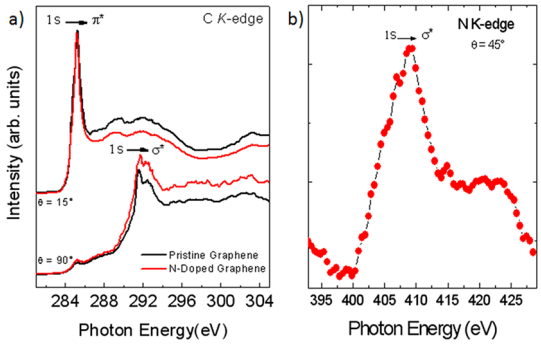

Figure 5. (a) Carbon *K*-edge NEXAFS spectra of pristine (black line) and N-doped graphene (red line), measured for various angles of X-ray incidence. The features at 285.2 and 291.5 eV are attributed to the 1s→π* and 1s→σ* transitions, respectively. (b) Nitrogen *K*-edge NEXAFS spectrum for the N-doped graphene.

are shown in Figure 5a. In both samples, we find spectral fingerprints of sp^2-hybridized carbon: the strong peaks at 285.4 and 292.0 eV correspond to the transition of a C 1s electron to the unoccupied π and σ orbitals, respectively.[26,37] The sharpness of the NEXAFS features indicates a well-defined bonding environment and a long-range periodic order in the electronic structure. The σ fine structure is specifically characteristic of graphite and includes a sharp onset due to an excitonic core hole valence state interaction, while the broader peak at 1 eV higher photon energy is due to more delocalized σ states. Thus, the NEXAFS spectra unequivocally prove the formation of sp^2 bonds between carbon atoms in both the pristine and the N-doped

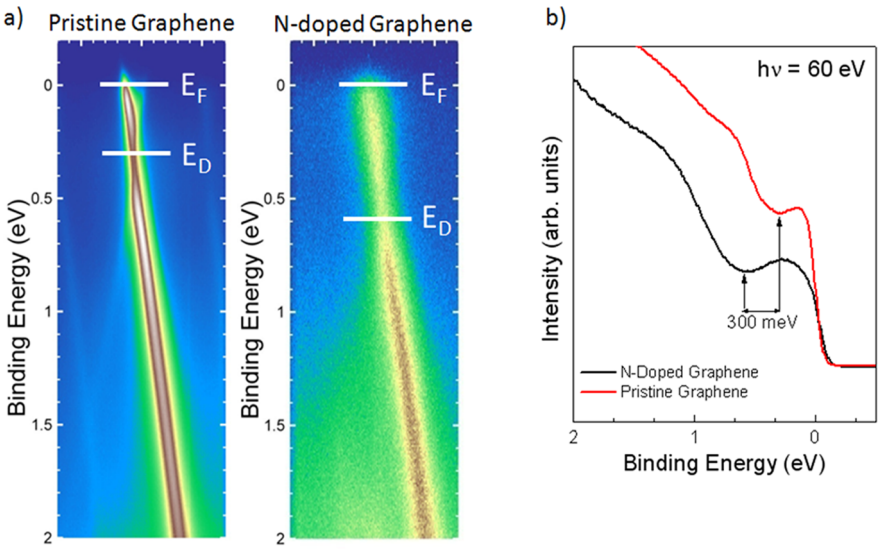

Figure 6. (a) ARPES at room temperature of pristine graphene and N-doped graphene/SiC(0001), measured at $h\nu$ = 60 eV, through the *K* point, along the ΓK direction. (b) ARPES intensity integrated spectra as a function of the binding energy, extracted from the 2D ARPES map, for the initial pristine graphene (red line) and N-doped graphene (black line).

graphene. As the electronic structure primarily depends on local coordination, this shows that the coordination of N is similar to C for each composition. The normalized N *K*-edge NEXAFS spectrum, however, shows a small σ^* peak and the absence of π^* feature (Figure 5b). Following the work of Robertson *et al.*, we interpret this as a signature of Si−N−C bonds due to nitrogen atoms penetrating into the substrate.[38] We cannot infer on the substitution of C atoms by N in the graphene layer based on these data since the π^* feature could well be too small to measure and rely on XPS data to conclude on this point.[39]

We studied the influence of N-doping on the electronic structure of graphene with ARPES. The band structures of pristine and N-doped graphene, collected at the *K* point along the ΓK direction, are shown in Figure 6a,b, respectively. For the pristine graphene, the Dirac crossing point of the π band is located around 0.3 eV below the Fermi level. This n-type doping is typical of epitaxial graphene and is due to the charge transfer from SiC substrate. For N-doped graphene, the Dirac point is shifted by 0.3 eV toward higher binding energies with respect to the π band of pristine graphene. This increase of the n-type doping of graphene can be explained as the result of charge transfer from nitrogen atoms to the graphene layer. Having determined the position of the Dirac point, the carrier concentration of the graphene can be estimated as $|N| = (E_F - E_D)^2/\pi(\hbar v_F)^2$, where N is the electron density, $v_F = 1 \times 10^6$ m/s is the Fermi velocity of graphene, E_F (E_D) is the energy position of the Fermi level (energy of the Dirac point).[4,40,41] We find for the electron density of the pristine graphene a value of about 6.6×10^{12} cm^{-2}. For the N-doped graphene layer, the carrier concentration is estimated to be around 2.6×10^{13} cm^{-2}, suggesting an effective electron doping of the epitaxial graphene despite a small amount of nitrogen dopants. The difference in the electron density between the pristine and N-doped graphene of about 2×10^{13} cm^{-2} is due to the incorporation of N atoms, and it is worthwhile noticing that this doping effect is mainly due to the graphitic configuration. In the following, we neglect the influence of pyridinic and pyrrolic nitrogen on the carrier concentration of N-doped graphene since their theoretically predicted doping effect is much weaker than in the case of graphitic nitrogen.[25] Assuming that the N-graphitic atom gives one electron per atom, the observed change in the carrier concentration of 2×10^{13} cm^{-2} is a direct estimation of the amount of N-graphitic atoms per unit area. As the area density of C atoms in the graphene is 3.8×10^{15} cm^{-2}, the graphitic nitrogen atom density is 0.5%, in excellent agreement with what was found in our XPS experiment.

CONCLUSIONS

In summary, we have developed a methodology to synthesize monolayer nitrogen-doped graphene using a growth process under N_2 and Si flux. This *in situ* doping method is highly attractive for the efficient incorporation of doping species into the graphene lattice. The epitaxial N-graphene layers were evidenced by LEEM, HR-TEM, and Raman measurements. XPS and ARPES spectroscopy established that the process resulted in in-plane nitrogen substitution in the monolayer graphene. The doping was confirmed by further ARPES measurements, which clearly shows n-type sample behavior. Graphitic-like nitrogen atoms induce a large increase of the charge density in the graphene layers. The production and the characterization of such large-scale N-doped graphene on SiC is a

first step toward an oxygen reduction reaction, which could have potential application in the fabrication of other low-dimensional nanostructures with desired functionalities.

METHODS

Graphene was grown on 4H-SiC(0001) undoped wafers. The substrate was first etched in a hydrogen flux at 1500 °C at 200 mbar for 15 min in order to remove any damage caused by surface polishing and to form a step-ordered structure on the surface. After the etching, the substrate was transferred into an ultrahigh vacuum (UHV) chamber with a base pressure of 10^{-9} mbar. The surface of the substrate was degassed by an annealing at 600 °C. The substrates were heated under a Si flux (1 ML/min) at 800 °C to remove the native oxide in UHV ($P = 2 \times 10^{-9}$ mbar). Graphene growth was carried out in a chamber equipped with a solid Si source and a LEED system. Graphene was synthesized by exposing the substrate to a nitrogen (N_2) and Si flux at 1200−1400 °C under semi-UHV ($P = 2 \times 10^{-5}$ mbar) (first 5 min under N_2 and Si flux and second 5 min under N_2). This induces a growth of a (3×3), $(\sqrt{3} \times \sqrt{3})R30°$, and $(6\sqrt{3} \times 6\sqrt{3})R30°$ reconstructions as an intermediate step toward few-layer growth of graphene due to Si depletion. After growth of the graphene layer, the sample was quenched to 500 °C under nitrogen flux. The nitrogen was introduced into the chamber through a variable leak valve. The temperature of the substrate was calibrated with an infrared pyrometer in the high-temperature range and with a thermocouple in the low-temperature range. After graphitization, the sample was characterized with HR-TEM, LEEM, XPS, and ARPES techniques.

LEEM measurements were carried at room temperature (Elmitec GmBH-LEEM III) with a spatial resolution better than 30 nm at the CEA/IRAMIS/SPCSI laboratory (Saclay, France). The bias difference between the electron gun and sample was the start voltage and was roughly equal to the primary electron beam energy. The micro-Raman spectroscopy was performed at room temperature with a Renishaw spectrometer using 514 nm laser light focused on the sample by a DMLM Leica microscope with a 100× (NA = 0.75) objective and a power of 5 mW with a spot size of about 1 μm.

High-resolution core level X-ray and angle-resolved photoelectron spectroscopy and X-ray absorption with synchrotron radiation were carried out at the third generation SOLEIL storage ring operated in the top-up mode at 300 mA, using the photoemission end station of the TEMPO beamline (Saint-Aubin, France), which covers an energy range of 50−1500 eV. The experiments were performed at room temperature with a base pressure of 2×10^{-10} mbar. Photoelectrons were analyzed at a takeoff angle of 90° with respect to the sample surface using a Scienta SES 2002 hemispherical analyzer and a delay line detector. NEXAFS provides a direct, element-specific probe of bond type and orientation with a high surface sensitivity that enables evaluation of sp^2:sp^3 bond ratios and the degree of planarity for single-layer films.

Measurements were performed in carbon Auger peak mode, selected to optimize the surface sensitivity of the measurement and thereby the signal from the graphene film. Angle-dependent NEXAFS was obtained by changing the angle between the incoming X-ray beam (and therefore the E-field vector) and the sample between 5 and 85°, corresponding roughly to out-of-plane and in-plane bond resonances, respectively. The reference absorption intensity (I_0) of the incoming X-ray beam (Si 2p of SiC substrates) was measured simultaneously and used to normalize the spectra to avoid any artifacts due to beam instability. For ARPES measurements, the photon energy ($h\nu$ = 60 eV) and sample orientation were set in order to explore the k-space region around the K point in the ΓK direction of the Brillouin zone. Prolonged air exposure, however, leads to a fractional layer of physisorbed hydrocarbons and water, which were removed by annealing in vacuum ($P = 2 \times 10^{-9}$ mbar) at around 600 °C (30 min).

Conflict of Interest: The authors declare no competing financial interest.

Acknowledgment. We are grateful to M. Eddrief, B. Etienne, M. Ridene, and L. Travers for fruitful discussions, and G. Patriache for the TEM experiments. This work was supported by the French Contracts ANR-2010-MIGRAQUEL and ANR-2011-SUPERTRAMP, and the RTRA Triangle de la Physique.

REFERENCES AND NOTES

1. Novoselov, K. S.; Geim, A. K.; Morozov, S. V.; Jiang, D.; Katnelson, M. I.; Grigorieva, I. V.; Dubonos, S. V.; Firsov, A. A. Two-Dimensional Gas of Massless Dirac Fermions in Graphene. *Nature* **2005**, *438*, 197–200.
2. Novoselov, K. S.; Jiang, Z.; Zhang, Y.; Morozov, S. V.; Stormer, H. L.; Zeitler, U.; Maan, J. C.; Boebinger, G. S.; Kim, P.; Geim, A. K. Room-Temperature Quantum Hall Effect in Graphene. *Science* **2007**, *315*, 1379–1379.
3. Betz, A. C.; Vialla, F.; Brunel, D.; Voisin, C.; Picher, M.; Cavanna, A.; Madouri, A.; Fève, G.; Berroir, J.-M.; Plaçais, B.; *et al.* Hot Electron Cooling by Acoustic Phonons in Graphene. *Phys. Rev. Lett.* **2012**, *109*, 056805.
4. Sprinkle, M.; Ruan, M.; Hu, Y.; Hankinson, J.; Rubio-Roy, M.; Zhang, B.; Wu, X.; Berger, C.; de Heer, W. A. Scalable Templated Growth of Graphene Nanoribbons on SiC. *Nat. Nanotechnol.* **2010**, *5*, 727–731.
5. Ouerghi, A.; Ridene, M.; Balan, A.; Belkhou, A.; Barbier, A.; Gogneau, N.; Portail, M.; Michon, A.; Latil, S.; Jegou, P.; *et al.* Sharp Interface in Epitaxial Graphene Layers on 3C-SiC-(100)/Si(100) Wafers. *Phys. Rev. B* **2011**, *83*, 205429.
6. Reddy, A. L. M.; Srivastava, A.; Gowda, S. R.; Gullapalli, H.; Dubey, M.; Ajayan, P. M. Synthesis of Nitrogen-Doped Graphene Films for Lithium Battery Application. *ACS Nano* **2010**, *4*, 6337–6342.
7. Qu, L.; Liu, Y.; Baek, J.-B.; Dai, L. Nitrogen-Doped Graphene as Efficient Metal-Free Electrocatalyst for Oxygen Reduction in Fuel Cells. *ACS Nano* **2010**, *4*, 1321–1326.
8. Balog, R .; Jorgensen, B.; Nilsson, L.; Andersen, M.; Rienks, M.; Bianchi, M.; Fanetti, M.; Lægsgaard, E.; Baraldi, A.; Lizzit, S.; *et al.* Bandgap Opening in Graphene Induced by Patterned Hydrogen Adsorption. *Nat. Mater.* **2010**, *9*, 315–319.
9. Kwon, O. S.; Park, S. J.; Hong, J. Y; Han, A. R.; Lee, J. S.; Lee, J. S.; Oh, J. H.; Jang, J. Flexible FET-Type VEGF Aptasensor Based on Nitrogen-Doped Graphene Converted from Conducting Polymer. *ACS Nano* **2012**, *6*, 1486–1493.
10. Zhao, W.; Höfert, O.; Gotterbarm, K.; Zhu, J. F.; Papp, C.; Steinrück, H. P. Production of Nitrogen-Doped Graphene by Low-Energy Nitrogen Implantation. *J. Phys. Chem. C* **2012**, *116*, 5062.
11. Schiros, T.; Nordlund, D.; Pálová, L.; Prezzi, D.; Zhao, L.; Soo Kim, K. S.; Wurstbauer, U.; Gutiérrez, C.; Delongchamp, D.; Cherno Jaye, C.; *et al.* Connecting Dopant Bond Type with Electronic Structure in N-Doped Graphene. *Nano Lett.* **2012**, *12*, 4025–4031.
12. Zhao, L.; He, R.; Rim, K. T.; Schiros, T.; Kim, K. S.; Zhou, H.; Gutiérrez, C.; Chockalingam, S. P.; Arguello, C. J.; Palova, L.; *et al.* Visualizing Individual Nitrogen Dopants in Monolayer Graphene. *Science* **2011**, *333*, 999–1003.
13. Koch, R. J.; Weser, M.; Zhao, W.; Viñes, F.; Gotterbarm, K.; Kozlov, S. M.; Höfert, O.; Ostler, M.; Papp, C.; Gebhardt, J.; *et al.* Growth and Electronic Structure of Nitrogen-Doped Graphene on Ni(111). *Phys. Rev. B* **2012**, *86*, 075401.
14. Usachov, D.; Vilkov, O.; Grüneis, A.; Haberer, D.; Fedorov, A.; Adamchuk, V. K.; Preobrajenski, A. B.; Dudin, P.; Barinov, A.; Oehzelt, M.; *et al.* Nitrogen-Doped Graphene: Efficient

Growth, Structure, and Electronic Properties. *Nano Lett.* **2011**, *11*, 5401–5407.
15. Deifallah, M.; McMillan, P. F.; Cora, F. Electronic and Structural Properties of Two-Dimensional Carbon Nitride Graphenes. *J. Phys. Chem. C* **2008**, *112*, 5447–5453.
16. Gong, K.; Du, F.; Xia, Z.; Duratock, M.; Dai, L. Nitrogen-Doped Carbon Nanotube Arrays with High Electrocatalytic Activity for Oxygen Reduction. *Science* **2009**, *323*, 760–764.
17. Wang, Y.; Shao, Y.; Matson, D. W.; Li, J.; Lin, Y. Nitrogen-Doped Graphene and Its Application in Electrochemical Biosensing. *ACS Nano* **2010**, *4*, 1790–1798.
18. Podila, R.; Chacon-Torres, J.; Spear, J. T.; Pichler, T.; Ayala, P.; Rao, A. M. Spectroscopic Investigation Of Nitrogen Doped Graphene. *Appl. Phys. Lett* **2012**, *101*, 123108.
19. Brenner, K.; Murali, R. *In Situ* Doping of Graphene by Exfoliation in a Nitrogen Ambient. *Appl. Phys. Lett.* **2011**, *98*, 113115.
20. Imamura, G.; Saiki, K. Synthesis of Nitrogen-Doped Graphene on Pt(111) by Chemical Vapor Deposition. *J. Phys. Chem. C* **2011**, *115*, 10000–10005.
21. Sheng, Z. H.; Lin Shao, L.; Chen, J. J.; Bao, W. J.; Wang, F. B.; Xia, X. H. Catalyst-Free Synthesis of Nitrogen-Doped Graphene *via* Thermal Annealing Graphite Oxide with Melamine and Its Excellent Electrocatalysis. *ACS Nano* **2011**, *5*, 4350–4358.
22. Guo, B.; Liu, Q.; Chen, E.; Zhu, H.; Fang, L.; Gong, J. R. Controllable N-Doping of Graphene. *Nano Lett.* **2010**, *10*, 4975–4980.
23. Wei, D.; Liu, Y.; Wang, Y.; Zhang, H.; Huang, L.; Yu, G. Synthesis of N-Doped Graphene by Chemical Vapor Deposition and Its Electrical Properties. *Nano Lett.* **2009**, *9*, 1752–1758.
24. Emtsev, K. V.; Bostwick, A.; Horn, K.; Jobst, J.; Kellogg, G. L.; Ley, L.; McChesney, J. L.; Ohta, T.; Reshanov, S. A.; Röhrl, J.; *et al.* Towards Wafer-Size Graphene Layers by Atmospheric Pressure Graphitization of Silicon Carbide. *Nat. Mater.* **2009**, *8*, 203–207.
25. Joucken, F.; Tison, H.; Lagoute, J.; Dumont, J.; Cabosart, D.; Zheng, B.; Repain, V.; Chacon, C.; Girard, Y.; Botello-Mendez, A. R.; *et al.* Localized State and Charge Transfer in Nitrogen-Doped Graphene. *Phys. Rev. B* **2012**, *85*, 161408(R).
26. Ouerghi, A.; Silly, M. G.; Marangolo, M. C.; Eddrief, M.; Picher, M.; Sirotti, F.; El Moussaoui, S.; Belkhou, R. Large Area and High-Quality Epitaxial Graphene on Off-Axis SiC Wafers. *ACS Nano* **2012**, *6*, 6075–6082.
27. Ouerghi, A.; Belkhou, R.; Marangolo, M.; Silly, M. G.; El Moussaoui, S.; Eddrief, M.; Largeau, L.; Portail, M.; Sirotti, F. Structural Coherency of Epitaxial Graphene on 3C-SiC-(111) Epilayers on Si(111). *Appl. Phys. Lett.* **2010**, *97*, 161905.
28. Ni, Z. H.; Chen, W.; Fan, X. F.; Kuo, J. L.; Yu, T.; Wee, A. T. S.; Shen, Z. X. Raman Spectroscopy of Epitaxial Graphene on a SiC Substrate. *Phys. Rev. B* **2008**, *77*, 115416.
29. Ferrari, A. C. Raman Spectroscopy of Graphene and Graphite: Disorder, Electron−Phonon Coupling, Doping and Nonadiabatic Effects. *Solid State Commun.* **2007**, *143*, 47–57.
30. Ferralis, N.; Maboudian, R.; Carraro, C. Evidence of Structural Strain in Epitaxial Graphene Layers on 6H-SiC(0001). *Phys. Rev. Lett.* **2008**, *101*, 156801.
31. Riedl, C.; Coletti, C.; Starke, U. Structural and Electronic Properties of Epitaxial Graphene on SiC(0001): A Review of Growth, Characterization, Transfer Doping and Hydrogen Intercalation. *J. Phys. D: Appl. Phys.* **2010**, *43*, 374009.
32. Cancado, L. G.; Takai, K.; Enoki, T.; Endo, M.; Kim, Y.; Mizusaki, H.; Jorio, A.; Coelho, L. N.; Magalhaes-Paniago, R.; Pimenta, M. A. General Equation for the Determination of the Crystallite Size La of Nanographite by Raman Spectroscopy. *Appl. Phys. Lett.* **2006**, *88*, 163106.
33. Kim, J. W.; Yeom, H. W. Surface and Interface Structures of Epitaxial Silicon Nitride on Si(111). *Phys. Rev. B* **2003**, *67*, 035304.
34. Chai, J. W.; Pan, J. S.; Zhang, Z.; Wang, S. J.; Chen, Q.; Huan, C. H. A. X-ray Photoelectron Spectroscopy Studies of Nitridation on 4H-SiC (0001) Surface by Direct Nitrogen Atomic Source. *Appl. Phys. Lett.* **2008**, *92*, 092119.
35. Sun, G. F.; Liu, Y. S.; Rhim, H.; Jia, J. F.; Xue, Q. K.; Weinert, M.; Li, L. Si Diffusion Path for Pit-Free Graphene Growth on SiC(0001). *Phys. Rev. B* **2011**, *84*, 195455.
36. Yeh, J. J.; Lindau, I. Atomic Subshell Photoionization Cross-Sections and Asymmetry Parameters. *At. Data Nucl. Data Tables* **1985**, *32*, 1–155.
37. Aristov, V. Y.; Urbanik, G.; Kummer, K.; Vyalikh, D. V.; Molodtsova, O. V.; Preobrajenski, A. B.; Zakharov, A. A.; Hess, C.; Hanke, T.; Buchner, B.; *et al.* Graphene Synthesis on Cubic SiC/Si Wafers: Perspectives for Mass Production of Graphene-Based Electronic Devices. *Nano Lett.* **2010**, *10*, 992–995.
38. Robertson, J.; Davis, C. A. Nitrogen Doping of Tetrahedral Amorphous Carbon. *Diamond Relat. Mater.* **1995**, *4*, 441–444.
39. Shimoyama, I.; Wu, G.; Sekiguchi, T.; Baba, Y. Evidence for the Existence of Nitrogen-Substituted Graphite Structure by Polarization Dependence of Near-Edge X-ray-Absorption Fine Structure. *Phys. Rev. B* **2000**, *62*, R6053.
40. Pallecchi, E.; Ridene, M.; Kazazis, D.; Mathieu, C.; Schopfer, F.; Poirier, W.; Mailly, D.; Ouerghi, A. Observation of the Quantum Hall Effect in Epitaxial Graphene on SiC(0001) with Oxygen Adsorption. *Appl. Phys. Lett.* **2012**, *100*, 253109.
41. Mathieu, C.; Lalmi, B.; Mentes, T. O.; Pallecchi, E.; Locatelli, A.; Latil, S.; Belkhou, R.; Ouerghi, A. Effect of Oxygen Adsorption on the Local Properties of Epitaxial Graphene on SiC(0001). *Phys. Rev. B* **2012**, *86*, 035435.